RAA 2016 Vol. **16** No. **10**, 161 (8pp) doi: 10.1088/1674–4527/16/10/161
http://www.raa-journal.org *http://iopscience.iop.org/raa*

***R**esearch in*
***A**stronomy and*
***A**strophysics*

On the power-law distributions of X-ray fluxes from solar flares observed with *GOES*

You-Ping Li, Li Feng, Ping Zhang, Si-Ming Liu and Wei-Qun Gan

Key Laboratory of Dark Matter and Space Astronomy, Purple Mountain Observatory, Chinese Academy of Sciences, 210008 Nanjing, China; *yplee@pmo.ac.cn; liusm@pmo.ac.cn*

Received 2016 March 2; accepted 2016 June 30

Abstract The power-law frequency distributions of the peak flux of solar flare X-ray emission have been studied extensively and attributed to a system having self-organized criticality (SOC). In this paper, we first show that, so long as the shape of the normalized light curve is not correlated with the peak flux, the flux histogram of solar flares also follows a power-law distribution with the same spectral index as the power-law frequency distribution of the peak flux, which may partially explain why power-law distributions are ubiquitous in the Universe. We then show that the spectral indexes of the histograms of soft X-ray fluxes observed by *GOES* satellites in two different energy channels are different: the higher energy channel has a harder distribution than the lower energy channel, which challenges the universal power-law distribution predicted by SOC models and implies a very soft distribution of thermal energy content of plasmas probed by the *GOES* satellites. The temperature (T) distribution, on the other hand, approaches a power-law distribution with an index of 2 for high values of T. Hence the application of SOC models to the statistical properties of solar flares needs to be revisited.

Key words: Sun: flares — Sun: X-rays, Gamma rays — methods: statistical

1 INTRODUCTION

Power-law frequency distributions exist ubiquitously in nature, such as in the magnitude of earthquakes (Gutenberg & Richter 1954) or the frequency that a particular word is used in literature (Zipf 1949). More frequency distributions following a power law can be found in Clauset et al. (2009) and Aschwanden (2011). For a power-law frequency distribution, the number of events dN scales with the magnitude of the event $x(> 0)$ as a power-law function

$$dN = Ax^{-\delta}dx\,, \tag{1}$$

where the coefficient $A > 0$ and the power-law index δ is constant. Usually the distribution deviates from a power-law function towards the low end of the magnitude x. This deviation can be attributed either to the breakdown of the power-law scaling or to some observational bias (Li et al. 2013).

There have been quite a number of statistical works on X-ray emission from solar flares. The X-ray peak flux has a power-law frequency distribution with a power-law index varying from 1.6 to 2.1 for different studies (e.g., Hudson et al. 1969; Drake 1971; Shimizu 1995; Lee et al. 1995; Feldman et al. 1997; Shimojo & Shibata 1999; Veronig et al. 2002; Yashiro et al. 2006; Aschwanden & Freeland 2012). Without background subtraction, Veronig et al. (2002) found that the peak soft X-ray (SXR) flux of flares obeys a power-law distribution over three orders of magnitude from the flare *GOES* classes of C2.0 to X20. Feldman et al. (1997) divided flares observed by the *GOES* satellites into different groups according to the background level and used the background-subtracted peak flux of flares for statistics. They found that the power-law distribution can be extended down to A1.0 class flares. Based on the aforementioned statistical studies, Aschwanden & Freeland (2012) summarized, in their table 2, the total number of flares observed by the *GOES* satellites, the flux range where the frequency distribution is consistent with a power law, and the corresponding power-law indices. They found that these observations can be explained with a fractal-diffusive avalanche model (Aschwanden 2012; Du 2015).

Although the peak flux of large flares can be easily obtained due to their high values, the value of the peak flux for small flares is always contaminated by background emission, instrumental noise and potential flare identification bias. The latter can be overcome by using the histogram of flare flux, which incorporates properties of the light curve with the peak flux distribution, to study the related statistics. Zhang & Liu (2015) recently showed that the characteristics of the SXR light curve do not vary with

the value of the peak flux. The histogram of the flare flux is, therefore, intimately related to the peak flux distribution.

A series of *GOES* satellites have taken a huge amount of SXR flux measurements of the Sun over a span of 40 years. In this paper, the data obtained from 1981 to 2012 are used. Moreover, to reduce the effect of selection bias, instead of identifying individual flares, we will include all data points at an original *GOES* time cadence of 3 s before 2009 and 2 s after 2009 to study the statistics of differential histograms of the *GOES* fluxes, which are different from but intimately connected to the frequency distribution of the *GOES* peak fluxes studied before. The *GOES* data reduction is presented in Section 2. The histograms are shown in Section 3. In Section 4, we explore the origin of the power-law distribution of the differential histograms and its deviation from a power law towards the low value end of the flux. Conclusions and discussions are presented in Section 5.

2 *GOES* DATA REDUCTION

Since 1974, a series of *GOES* satellites have been put into operation and continuously measured the total SXR emission flux at two wavelengths: 1–8 Å and 0.5–4 Å. The time cadence was 3 s before 2009 December 1 and was improved to 2 s afterwards. More information on *GOES* data can be found in Aschwanden & Freeland (2012) and references therein. High temporal-resolution *GOES* data from 1981 to 2012 are used in this study.

Before carrying out detailed investigation, one needs to treat the caveats in the obtained data properly. Two types of anomalies in the *GOES* data are illustrated in Figure 1. In the left panels, the sudden drop of the flux from 04:36 to 05:38 UT is due to the entry of the satellite into the shadow of the Earth. To remove the effect of such data on the histogram of the flux, we identify local minimums of the flux associated with Earth occultations and ignore 150 data points before and 60 data points after these minimums.

The right panels show the other type of anomaly due to instrumental saturation (Ryan et al. 2012). The saturated data are marked by shaded regions from 19:42 to 19:59 UT. This type of anomaly only affects the histogram at extremely-high flux values, which can be readily identified in the histogram. In total, there are more than 322 million data points in our sample.

3 OBSERVATIONAL RESULTS

Panel (a) of Figure 2 shows the differential histograms of these fluxes in two energy channels. It is evident that the differential histograms of the fluxes follow a power-law distribution towards the high value end of these fluxes. With the maximum likelihood fitting procedure (Crosby et al. 1993; Clauset et al. 2009; Li et al. 2012), we fitted each histogram with a power-law model. The power-law index for the lower energy band is bigger than that of the higher energy channel. The spikes at the high value end of the fluxes are caused by the flux saturation mentioned above and have been excluded in our fitting. Panels (b-d) in Figure 2 are the histograms of a subset of the sample obtained with different sampling cadences, which have the same distribution as the complete sample.

To investigate the variation of the histograms in the solar cycle, different panels in Figure 3 show the histograms of the flux observed in different years. Although the power-law indexes show significant variation with time, the index for the low energy band is always bigger than that for the high energy band. Except in 2005 during solar minimum, the index in the low energy band is always greater than 2, which is consistent with the frequency distribution of the peak flux (Aschwanden & Freeland 2012).

4 INTERPRETATION OF THESE HISTOGRAMS

SXR emission observed by the *GOES* satellites is mostly produced via the thermal bremsstrahlung process with flux density given by

$$F(e) \propto \mathrm{EM}\, T^{-1/2} \exp(-e/k_{\mathrm{B}}T)\,, \tag{2}$$

where T, EM and e represent the plasma temperature, emission measure and photon energy, respectively and k_{B} is the Boltzmann constant. The observed power-law distribution of SXR fluxes in different energy bands can be used to derive the frequency distribution of T and EM.

From the fact that $F(e_l)^{-\delta_l}\mathrm{d}F(e_l) \propto F(e_h)^{-\delta_h}\mathrm{d}F(e_h)$, where e_l, e_h and δ_l, δ_h represent the high- and low-energy bands and the corresponding power-law indexes of their histograms, respectively, we have

$$\begin{aligned}&[\mathrm{EM}\, T^{-1/2} \exp(-e_l/k_{\mathrm{B}}T)]^{1-\delta_l} \\ &\propto [\mathrm{EM}\, T^{-1/2} \exp(-e_h/k_{\mathrm{B}}T)]^{1-\delta_h}\end{aligned} \tag{3}$$

$$\begin{aligned}\mathrm{EM} \;&\propto\; T^{1/2} \\ &\times \exp\{[(\delta_l-1)e_l-(\delta_h-1)e_h]/[k_{\mathrm{B}}T(\delta_l-\delta_h]\}\end{aligned} \tag{4}$$

$$F(e_l) \;\propto\; \exp\{[(\delta_h-1)(e_l-e_h)]/[k_{\mathrm{B}}T(\delta_l-\delta_h]\}\,, \tag{5}$$

$$F(e_h) \;\propto\; \exp\{[(\delta_l-1)(e_l-e_h)]/[k_{\mathrm{B}}T(\delta_l-\delta_h]\}\,, \tag{6}$$

and the frequency distribution of T is then given by

$$\begin{aligned}D(T) &\propto T^{-2} \\ &\times \exp\{[(\delta_l-1)(\delta_h-1)(e_h-e_l)]/ \\ &\quad [k_{\mathrm{B}}T(\delta_l-\delta_h)]\}\,.\end{aligned} \tag{7}$$

The frequency distribution of $\mathrm{EM}T^{-1/2}$ follows a power law with an index of $\alpha = [\delta_l(\delta_h-1)e_h - \delta_h(\delta_l-1)e_l]/[(\delta_h-1)e_h-(\delta_l-1)e_l] \geq \delta_l$. If $\delta_l = \delta_h$, then $\alpha = \delta_l$, and Equation (2) implies that T needs to be a constant. Therefore different spectral indexes for the histograms of low and high channels are intimately related to the temperature distribution and the correlation between T

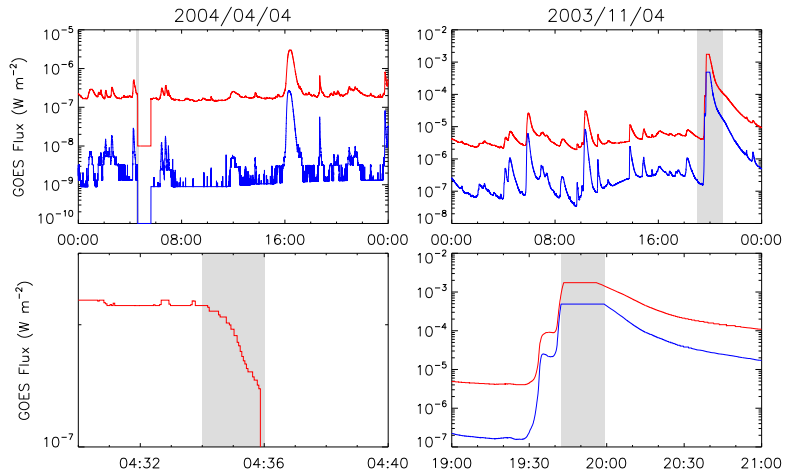

Fig. 1 Two types of anomalies in the *GOES* data. *Left panels*: sudden drop of flux due to Earth occultation; *Right panels*: instrumental flux saturation.

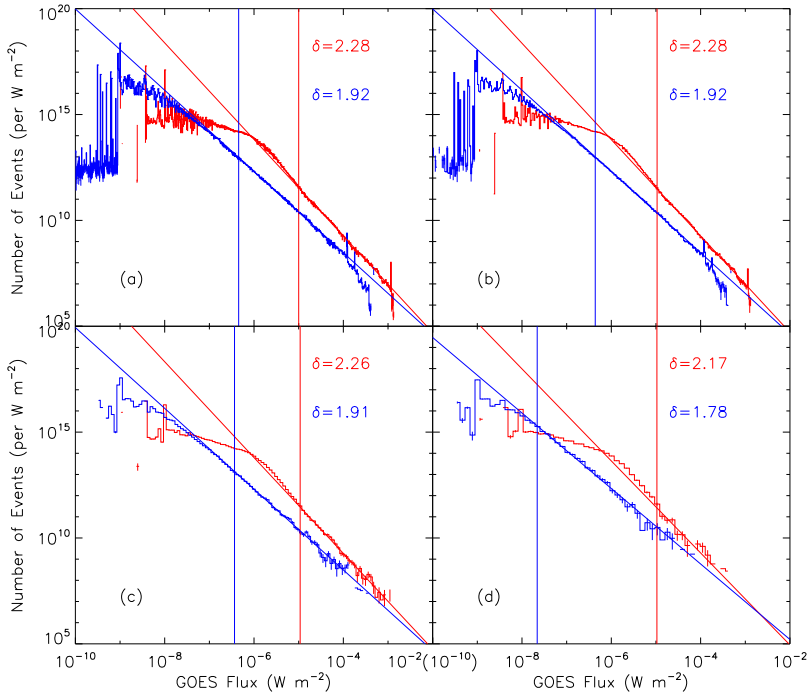

Fig. 2 Differential histograms of the original data and those with coarser samplings. Red is for the 1–8 Å *GOES* flux and blue is for the 0.5–4 Å flux. The fittings of these histograms with a power-law model (Clauset et al. 2009) are indicated with straight lines with the indexes given in the corresponding figures. The vertical lines mark the lower cutoffs of the corresponding power laws. Panel (a): histograms of the full sample; (b) histograms of the data sampled with a cadence of 1-minute/40-s (for a time resolution of 3 s and 2 s , respectively); (c) histograms of the data sampled with a cadence of 1-hour/40-minute; (d) histograms of the data sampled with a cadence of 1 day/16 hours.

and EM. Equations (5) and (6) show that the harder distribution of $F(e_h)$ is caused by the greater dependence of $F(e_h)$ on T than $F(e_l)$.

It is interesting to note that the temperature distribution $D(T)$ approaches a power-law distribution with an index of 2 at high values of T. The fast increase of the distribution toward low values of T may be attributed to contribution from the background plasma which is not necessarily associated with individual flare events. Then in self-organized criticality (SOC) models, one should associate quantities, which have a universal power-law distribution with an index of 2, with intensive variable T instead of fluxes or thermal energy, which are combinations of intensive and extensive variables.

Equation (7) shows that $1/T$ follows an exponential distribution with a cutoff of $[k_{\rm B}(\delta_l - \delta_h)]/(\delta_l - 1)(\delta_h -$

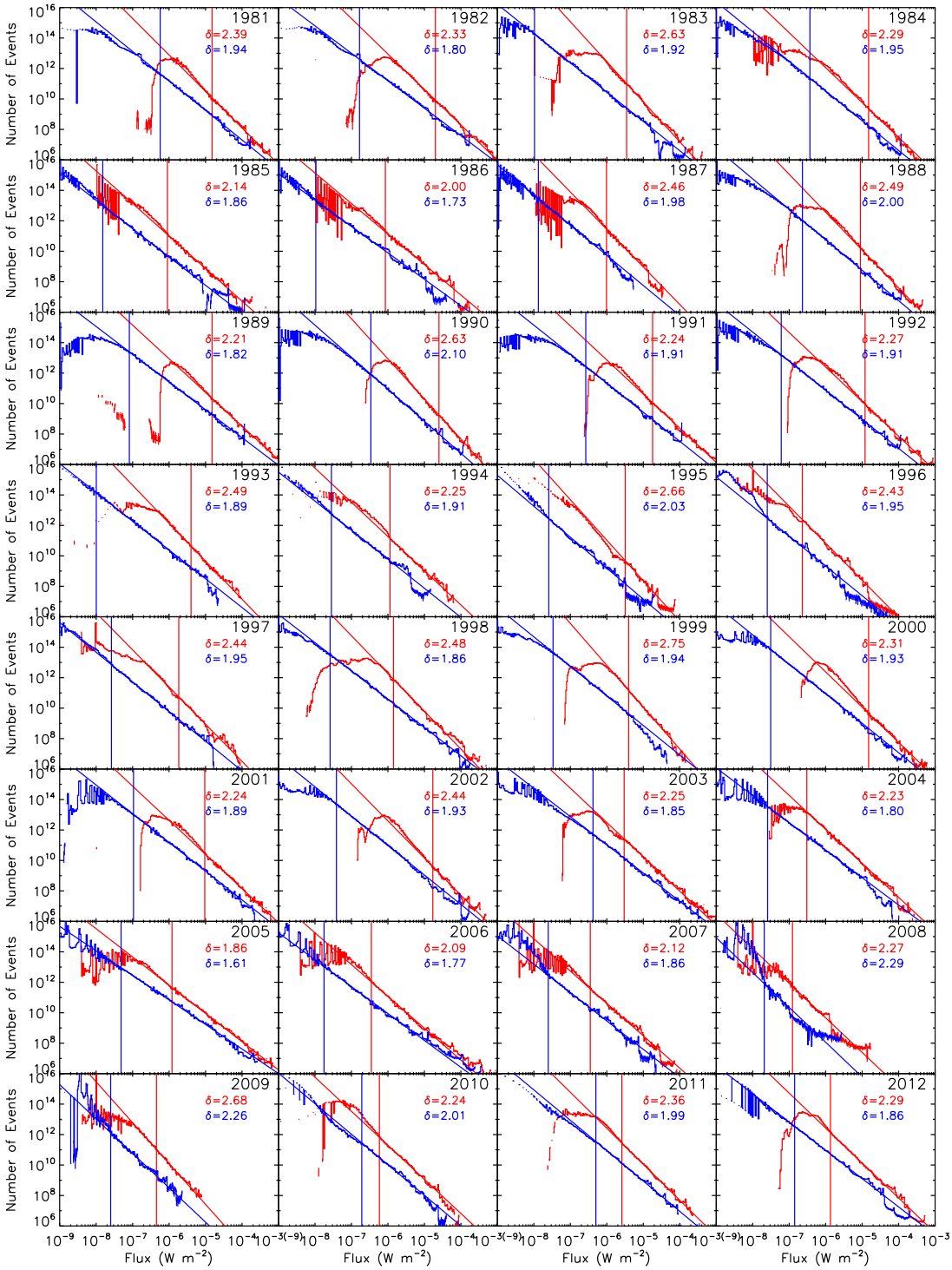

Fig. 3 The histograms and their corresponding fittings in each year from 1981 to 2012. The year is indicated in the upper-right corner in each panel. The colors and symbols have the same meanings as those in Fig. 2.

$1)(e_h - e_l)]$. The temperature of hot plasmas detected by the *GOES* satellites therefore is distributed in a relatively narrow range, which is consistent with results given by Ryan et al. (2012). Assuming that volume V of the emission region is not correlated with T and density n, which appears to be the case for existing solar flare observations (Li et al. 2012), the thermal energy of the emitting plasma is then proportional to $nVT \propto (\mathrm{EM}V)^{1/2}T$. Considering the narrow distribution of T, the thermal energy of the emitting plasma therefore follows a power-law distribution with an index of $2\alpha - 1 > 3$, where we have used the fact that $\alpha > \delta_l > 2$. Therefore, hot plasmas with a low energy

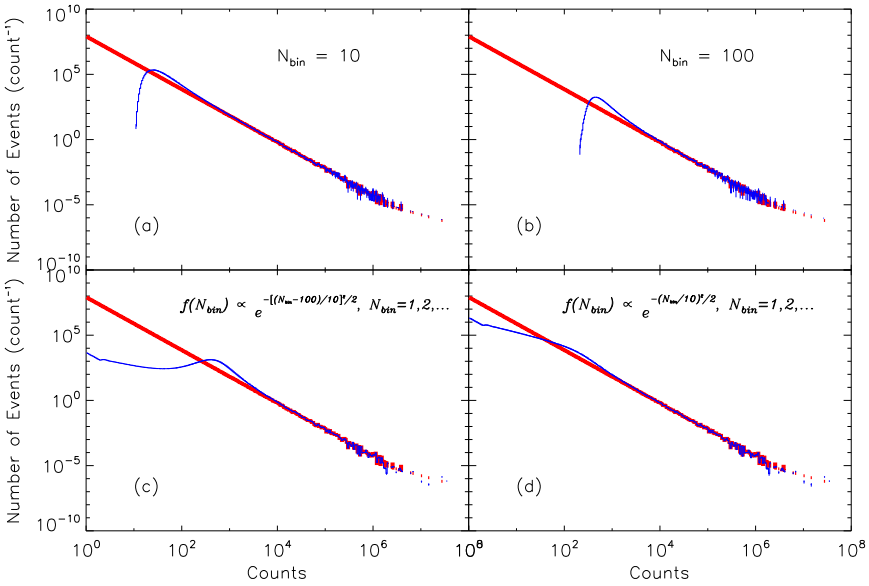

Fig. 4 A demonstration of the element superposition model. The original frequency distribution of the counts of elements is indicated in red in each panel. Panel (a): randomly selected $N_{\rm bin} = 10$ elements, and the sum of their counts that form a new event point. The blue curve is the frequency distribution of the counts of such a defined new event. Panel (b): Similar to the distribution in panel (a), but with $N_{\rm bin} = 100$. Panels (c) and (d): $N_{\rm bin}$ follows a Gaussian distribution as indicated at the top of the panel.

content dominate the thermal energy associated with flares (Hudson 1991).

One should emphasize that the histograms of *GOES* fluxes studied here are different from frequency distributions of the flare peak flux that are commonly investigated. However, if the time evolution of the flux is assumed to be independent of the peak flux

$$F = F_{\rm p} f(t) \ ,$$

where $0 < f(t) \leq 1.0$ and $f(0) = 1$ describe the statistically averaged time evolution of the normalized flare X-ray flux, and $F_{\rm p}$ is the peak flux at the peak time $t = 0$, the frequency distribution of the observed flux of a given flare is then given by

$$\frac{{\rm d}n(F)}{{\rm d}F} \equiv \left| \frac{{\rm d}t}{T{\rm d}F} \right| = \frac{f}{TFf'} \ ,$$

where T is the sampling interval, $f' = {\rm d}f/{\rm d}t$.

We note that the light curve of the normalized flux may vary drastically from one flare to another. However, as shown by Zhang & Liu (2015), the statistical properties of flare light curves indeed do not vary with $F_{\rm p}$. One may divide the light curve of the normalized flux of all flares into several groups depending on their level of similarity with each group represented by a characteristic light curve. $f(t)$ is then the weighted mean of these characteristic light curves. If $F_{\rm p}$ follows a power-law distribution with an index of δ above some cutoff frequency, the frequency distribution of F for all flares is then given by

$$\begin{aligned} \frac{{\rm d}N(F)}{{\rm d}F} &\propto \int_F^\infty F_p^{-\delta} {\rm d}F_{\rm p} \frac{{\rm d}n(F)}{{\rm d}F} \\ &= F^{-\delta} \int_1^\infty f(t)^{\delta+1} \frac{{\rm d}t(f)}{T{\rm d}f} {\rm d}\left(\frac{1}{f}\right) \ , \end{aligned}$$

which has the same spectral index as the distribution of $F_{\rm p}$.

The histograms studied above deviate from a power-law distribution toward the low value end of the flux. At a given time, *GOES* records the SXR flux coming from all features occurring in the solar disk. In fact when we check a full-disk image in SXR, such as an image observed by the Soft X-ray Telescope onboard YOHKOH (Tsuneta et al. 1991), we can see active regions, sometimes with flares superposed on them (e.g., Li et al. 2012), as well as bright points (e.g., Shimojo & Shibata 1999; Zhang et al. 2001), and other features. Therefore, each single datum we had in the sections above is actually the superposition of the flux from a number of elementary phenomena. For simplicity, we will call an elementary phenomenon an element from now on.

If we assume the frequency distribution of the flux/count from these elements follows the same power law, it would be interesting to know how the frequency distribution produced by the superposition of a number of elements appears. We started from an original power-law distribution with an index of $\delta = 2.03$, a total of 80 million elements, and with a lower cutoff of 1. This distribution is shown in Figure 4 by a thick red line. To obtain the blue curve in panel (a), we randomly selected 10 data points along the original power law in red, and summed their counts to form a new data point. We repeated this process $8 \times 10^7/N_{\rm bin}$ times, and obtained $8 \times 10^7/N_{\rm bin}$ samples. The frequency distribution of the counts in this new sample is indicated by the blue curve in Figure 4(a). One immediate finding is that after superposing 10 elements at each data point, a "bump" appears in the range of about 10 to 100 counts. In addition, the drop from the power-law distribution at the lower end is very rapid. If we increase

the value of $N_{\rm bin}$ to 100 as indicated in panel (b), the deviation from the power law occurs below a higher value at about 5×10^3 counts, and the "bump" also shifts rightward.

As the number of elements on the solar disk is not constant with time, we may assume that $N_{\rm bin}$ follows a Gaussian distribution. In panels (c) and (d), we adopt two Gaussian distributions as indicated in the upper region of both panels. When comparing the part of the distribution that deviates from the power law between cases of constant and non-constant $N_{\rm bin}$, we find the "bump" regions in panels (c) and (d) are less prominent, and do not have a rapid drop toward the low end like the cases in panels (a) and (b). Interestingly, such distributions in panels (c) and (d) have a similar shape to the distributions shown in Figure 2.

If we attribute the "bump" feature in the histogram to the superposition of elementary sources, we can expect that the histogram varies with solar activity. At solar activity maximum, there are more elementary sources on the disk that can be superposed for a measured *GOES* flux. But at solar activity minimum, the number of elements that can be superposed is much lower.

To classify the 32 years from 1981 to 2012 according to the level of solar activity, we used the flare occurrence rate provided by Aschwanden & Freeland (2012) as a criterion. Seven years that had a flare occurrence rate below 3000 per year are classified in the solar minimum group. They are 1985, 1986, 1995, 1996, 2007, 2008 and 2009. Six years had a flare rate above 15 000 per year and they belong to the solar maximum group. They are 1989, 1990, 1991, 2000, 2001 and 2002. The solar medium activity group has a flare rate between 8000 to 13 000 per year. We found that 1983, 1992, 1993, 1998, 2004 and 2011 could be included in this group.

In Figure 5, the histograms of *GOES* 1–8 Å flux at different levels of solar activity are illustrated. The curves in red, blue and magenta represent the histograms of the flux measured around the activity levels of maximum, minimum and medium, respectively. The green curve is the histogram of flux measured over the entire period. As a first step to compare the results among the periods of maximum, medium and minimum activity, we again applied the method in Clauset et al. (2009) to fit a power law to each curve. The best-fit power-law indices are presented in the upper right corner. The vertical lines mark the corresponding lower cutoffs of the power laws. These also indicate the position below which a "bump" appears. We also find that the "bump" at solar maximum is in a flux range about one order of magnitude larger than the "bump" region at solar minimum.

A more sophisticated fitting method is to use the element superposition model. The fitting parameters include the power-law index δ, the Gaussian center and width which describe the distribution of the superposition number $N_{\rm bin}$, a ratio to convert counts into *GOES* flux, and another parameter to convert the model frequency to the frequency of *GOES* flux. Therefore, there are five free parameters.

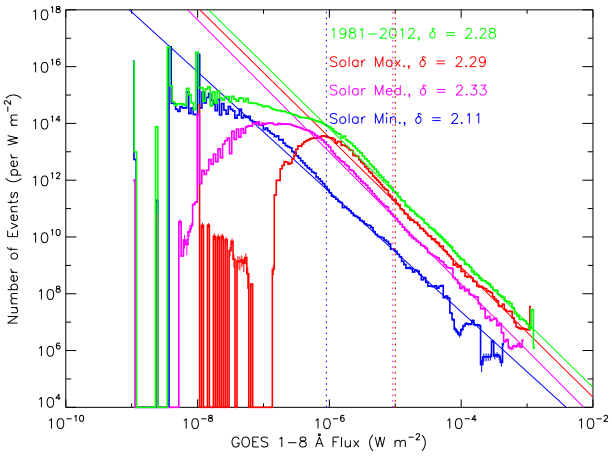

Fig. 5 Histograms of *GOES* 1–8 Å flux at different levels of solar activity. The curve in red shows the distribution of flux measured around the solar activity maximum. The curve in blue shows the result around the activity minimum. The one in magenta is the result derived from the flux at a medium activity level. The green one is the distribution of flux measured over the entire period from 1981 to 2012. The power-law indices of the fittings are indicated in the upper right corner, and vertical lines mark the lower cutoffs for flux.

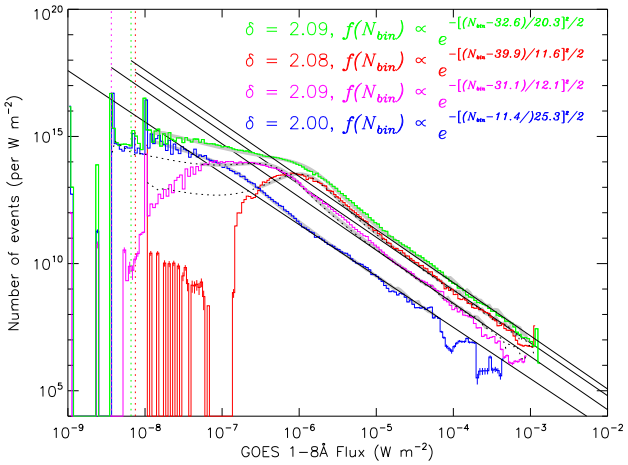

Fig. 6 Fittings of the element superposition model to the histograms of *GOES* 1–8 Å flux at different levels of solar activity. The colors have the same definition as those in Fig. 5. The solid gray lines indicate the results of the best-fit superposition models and their corresponding fitting ranges. The dashed lines represent the best-fit models to the histograms during the maximum and medium activities extrapolated down to lower flux values. The best-fit model parameters are marked in the upper-right region. The power-law distributions of the elementary phenomena are shown by the black solid lines with their lower cutoff marked by the vertical lines.

In Figure 6 the four histograms of *GOES* 1–8 Å flux during the periods of minimum, medium and maximum activity, and the entire 32 years are fitted with the element

superposition model using the non-linear least squares method. The best-fit power-law index and Gaussian parameters are marked in the upper right corner.

The black solid lines are the best-fit power laws for the elementary events. They can be extended down to the flux indicated by vertical lines, which could be regarded as the corresponding lower cutoffs. We can see that the lower cutoffs vary with the level of solar activity. This implies that the distribution of these elementary events also varies with the level of solar activity. The fittings in Figure 5 have power-law indices of 2.11, 2.33, 2.29 and 2.28 for the periods of solar activity corresponding to minimum, medium, maximum and the entire 32 years, whereas here the fittings of the superposition models in Figure 6 produce harder indices of 2.00, 2.09, 2.08 and 2.09, respectively.

It is interesting to note that the last three indices are consistent with each other, but the distinction between the first one and the others may be attributed to the inclusion of its data from all levels of solar activity. Furthermore, the power-law distributions of these new fittings cover much broader ranges of *GOES* flux of about five orders of magnitude from about 10^{-8} to $10^{-3}\,\mathrm{W\,m^{-2}}$.

The superposition model can fit the measured histograms fairly well. The thick gray lines in Figure 6 represent the results of the best-fit superposition models and their corresponding fitting ranges. For the *GOES* flux during the entire 32 years, the superposition model is able to fit the entire range of the histogram as indicated in green. For the *GOES* flux during solar minimum, the model produces higher values than the measured histogram at fluxes higher than $7 \times 10^{-5}\,\mathrm{W\,m^{-2}}$.

For the *GOES* flux during solar maximum and medium, the results of the best-fit models are delineated by two black dashed lines which are extrapolated down to lower flux values. The models have a higher number of events than the measured values close to the lower end. The deviation of the measured histogram at either the higher or lower flux end from the model may be due to selection bias when picking up the events occurring during the period of maximum, medium or minimum activity. The discrepancy at the lower flux end may also suggest the presence of an X-ray background during the solar active phases, which is distinct from the elementary events proposed above. The histogram in green takes into account all possible events occurring from 1981 to 2012. Therefore, it suffers the least influence of selection bias and produces the most convincing result.

When we compare the Gaussian peak value of N_{bin} in different activity periods, we find that it is proportional to the level of solar activity. Around solar maximum, the most probable N_{bin} is about 40. This value is larger than 31.1 from the medium activity period, and much larger than 11.4 from the solar minimum. These results could be understood as straightforward because the number of elements occurring on the solar disk increases with the level of solar activity.

5 CONCLUSIONS AND DISCUSSION

In this paper we have shown theoretically that if the shape of the flare light curve is not correlated with the peak flux, then the differential histogram of the flare flux shares the same power-law distribution as the frequency distribution of the peak flux. Observationally, we have investigated the statistics of all usable *GOES* 1–8 Å and 0.5–4 Å flux observed from 1981 to 2012 to minimize the effect of selection bias on frequency distributions. There are two major findings in our work.

(1) The histograms of two *GOES* channels obey power laws with different indices. The index of the power law for the 0.5–4 Å *GOES* flux is harder than the one for the 1–8 Å flux. These two indices do not change with the sampling cadence.
(2) A "bump"-like structure is clearly seen in all the histograms of the 1–8 Å flux. This could be interpreted by the element superposition model proposed in this paper. The original element frequency distribution of the entire 32-year data is a power law with an index of 2.09. This index is harder than the one derived from the fitting with the maximum likelihood method. The best-fit parameters of superposed sources N_{bin} are correlated with the level of solar activity.

The *GOES* 1–8 Å peak flux of flares without background subtraction has been found to follow a power law with an index greater than 2.1, e.g., Veronig et al. (2002) obtained an index of 2.11, and Yashiro et al. (2006) derived an index of 2.16. However, when the background is subtracted, the 1–8 Å peak flux of flares produced a harder index a bit below 2 (Lee et al. 1995; Feldman et al. 1997; Aschwanden & Charbonneau 2002). This difference between cases with and without background subtraction can possibly be interpreted by the element superposition model. The case with background subtractions is equivalent to the case with less superposed elements, as background subtraction would remove all other elementary sources other than flares. Actually, the frequency distribution of the background-subtracted flare peak flux could be linked to the upper portion of the distribution of elementary sources.

According to the theory of SOC (Aschwanden 2012), Aschwanden & Freeland (2012) predicted that the peak flux of flares in SXR has a power-law frequency distribution with an index of 2. From *GOES* 1–8 Å flux measurements, the frequency distributions of background-subtracted flare peak flux during 1975 to 2011 produced a power-law index of 1.98 ± 0.11 (Aschwanden & Freeland 2012). Our result of the power-law index of 2.09 (see Fig. 6) is a little bit softer than the theoretical value. The obtained power-law index in the 0.5–4 Å waveband using the maximum likelihood fitting method (see Fig. 2) is about 1.92. The single event in this waveband is also a superposition of a number of elementary sources. If we use the superposition model to derive the original element frequency distribution, we would probably get a power-law

index lower than 1.92, which was derived using the maximum likelihood method. As the "bump" structure is not very pronounced in this waveband, we did not use the superposition model for a further fitting. According to the SOC theory, the hard X-ray (HXR) peak flux of flares has a power-law index of 1.67. The emission from 0.5–4 Å probably contains some contribution from HXR. Therefore, the theoretical index might be between 1.67 and 2. Our power-law index of < 1.92 is consistent with the theoretical expectation. These results also indicate that the power-law distribution of X-ray fluxes from solar flares involves convolution of complex physical processes over a broad range of scales and may not be simply attributed to some scaling indexes of simple mathematical models.

We have to note that the power-law index of 2.09 we have is the statistical result over 32 years. We tried to minimize the bias of event selection, which can exist in flare statistics (Parnell & Jupp 2000; Aschwanden & Charbonneau 2002; Li et al. 2013). However, if we examine the distribution in each year as shown in Figure 3, then the power-law index for the 1–8 Å flux distribution ranges from 1.86 to 2.75, and for the 0.5–4 Å flux, it ranges from 1.61 to 2.29. Therefore, the power-law index is quite time dependent. In particular, in years 2005 and 2008, the power-law indices are very different from the values in other years.

In our simple element superposition model, the original power-law distribution has a lower cutoff of x_0. This is not a necessity, and other forms of lower-end deficiency can be used, such as saturation. As mentioned in the Introduction, 300 samples can cover the flux in two orders of magnitude with the power-law distribution using an index of 2. In principle, our 322 million data points can cover eight orders of magnitude associated with the data. However, in Figure 2 the apparent power law only covers two orders of magnitude. After removing the superposition effect, the frequency distributions of elementary sources could be able to cover five orders of magnitude associated with the data.

Due to the instrumental saturation of the very high *GOES* flux, we cannot know the exact upper limit of the flux. By extrapolating the frequency distribution of elementary sources to flux greater than $10^{-2}\,\mathrm{W\,m^{-2}}$ (equivalent to an X100 class flare), we find that this extremely high flux may occur 1000 times in 32 years. As our sampling frequency is 1/3 Hz most of the time, this corresponds to a time period of 3000 s, similar to the lifetime of a large flare. That is to say, we should be able to observe an X100 class flare within 32 years. Have we observed this kind of superflare? We do not know. It may be hidden in the saturated data.

Acknowledgements This work is supported partially by the Strategic Priority Research Program, the Emergence of Cosmological Structures, of the Chinese Academy of Sciences (Grant No. XDB09000000), MSTC Program 2011 CB811402, and the National Natural Science Foundation of China (NSFC) (Grant Nos. 11173063, 11173064, 11233008 and 11427803). L.F. is supported by the NFSC (Grant No. 11473070), and by the Natural Science Foundation of Jiangsu Province (Grant BK2012889). L.F. also acknowledges the Youth Innovation Promotion Association, CAS, for financial support.

References

Aschwanden, M. J., & Charbonneau, P. 2002, ApJ, 566, L59
Aschwanden, M. J. 2011, Self-Organized Criticality in Astrophysics: The Statistics of Nonlinear Processes in the Universe (Berlin: Springer-Praxis)
Aschwanden, M. J. 2012, A&A, 539, A2
Aschwanden, M. J., & Freeland, S. L. 2012, ApJ, 754, 112
Clauset, A., Shalizi, C. R., & Newman, M. E. J. 2009, SIAM Review, 51, 661
Crosby, N. B., Aschwanden, M. J., & Dennis, B. R. 1993, Sol. Phys., 143, 275
Drake, J. F. 1971, Sol. Phys., 16, 152
Du, Z. L. 2015, Ap&SS, 359, 4
Feldman, U., Doschek, G. A., & Klimchuk, J. A. 1997, ApJ, 474, 511
Gutenberg, B., & Richter, C. F. 1954, Seismicity of the Earth and Related Phenomena (2nd ed.; Princeton: Princeton Univ. Press), 310
Hudson, H. S., Peterson, L. E., & Schwartz, D. A. 1969, ApJ, 157, 389
Hudson, H. S. 1991, Sol. Phys., 133, 357
Lee, T. T., Petrosian, V., & McTiernan, J. M. 1995, ApJ, 448, 915
Li, Y. P., Gan, W. Q., & Feng, L. 2012, ApJ, 747, 133
Li, Y.-P., Gan, W.-Q., Feng, L., Liu, S.-M., & Struminsky, A. 2013, RAA (Research in Astronomy and Astrophysics), 13, 1482
Parnell, C. E., & Jupp, P. E. 2000, ApJ, 529, 554
Ryan, D. F., Milligan, R. O., Gallagher, P. T., et al. 2012, ApJS, 202, 11
Shimizu, T. 1995, PASJ, 47, 251
Shimojo, M., & Shibata, K. 1999, ApJ, 516, 934
Tsuneta, S., Acton, L., Bruner, M., et al. 1991, Sol. Phys., 136, 37
Veronig, A., Temmer, M., Hanslmeier, A., Otruba, W., & Messerotti, M. 2002, A&A, 382, 1070
Yashiro, S., Akiyama, S., Gopalswamy, N., & Howard, R. A. 2006, ApJ, 650, L143
Zhang, J., Kundu, M. R., & White, S. M. 2001, Sol. Phys., 198, 347
Zhang, P., & Liu, S.-M. 2015, Chin. J. Astron. Astrophys., 39, 330
Zipf, G. K. 1949, Human Behavior and the Principle of Least-Effort (Cambridge: Addison Wesley)